Simulation of Viscoelastic Coating Flows with a Volume-of-Fluid Technique

J Brethour
Flow Science, Inc., Santa Fe, New Mexico USA

Abstract

This work involves simulation of viscoelastic flows in coating processes. The basic computational approach uses a commercial CFD package, ***FLOW-3D***®[1] that uses a Volume-of-Fluid (VOF) technique along with a Fractional Area and Volume Representation of solid regions to simulate transient, free-surface flows within a structured, fixed mesh.

The viscoelastic model accepts a variety of constitutive equations. The approach taken uses the concept of a conformation tensor[2] to track the history of the rotation, stretching and relaxation of the fluid throughout the computational domain. Each conformation tensor component's history is tracked through the fixed grid flow domain. In this manner, large fluid deformations and even break-up can be computed without the need for remeshing. These computations are solved alongside the conservation of mass and momentum equations already present in the flow model. Additional parameters required are the elastic modulus, which controls the resistance to deformation of the individual molecules, and the relaxation time, which controls the rate at which the stretched molecules retract.

Computational results are compared with experimental results of the low-flow limit in slot coating[3] where the feed of coating liquid is gradually reduced until the downstream contact line becomes unstable. The viscosity and elastic properties of the fluid are varied. The computational results correlate well with experiments for both variations in Capillary number and elasticity of the fluid. Also, the effects of viscoelasticity on slide coating, spray coating and roll coating are explored.

Introduction

FLOW-3D® is a general-purpose computational fluid dynamics solver that is widely used in various industries to solve complex transient three-dimensional flow problems. It is especially convenient to solve free-surface problems because its Volume-of-fluid method (VOF) allows it to track accurately the shape and dynamics of the air-liquid interface, without the need to compute the dynamics of the gas phase. Within this solver has been implemented an elastic stress solver that builds upon the methods already incorporated into the code. In the work presented here, the elasticity model uses a conformation tensor approach to predict the orientation, stretching and relaxation of the solution molecules. From this conformation tensor is extracted the elastic stress.

Calculation of the Conformation tensor

Following on the Oldroyd-B model as proposed by Pasquali and Scriven[2], this work computes the update to the conformation tensor, **M**:

$$\frac{\partial \mathbf{M}}{\partial t} = \underbrace{-\mathbf{u}\cdot\nabla\mathbf{M}}_{\text{Change due to fluid motion}} + \underbrace{\nabla\mathbf{u}^T\cdot\mathbf{M} + \mathbf{M}\cdot\nabla\mathbf{u} + \nabla\mathbf{u} + \nabla\mathbf{u}^T}_{\text{Change due to stretching, orientation and rotation}} - \underbrace{\frac{1}{\lambda}\mathbf{M}}_{\text{Change due to relaxation}} . \qquad (1)$$

Here, the equilibrium value for the conformation tensor **M** is **0**, **u** is the local fluid velocity, and λ is the relaxation time of the material. The resulting value of **M** is used to compute the elastic stress tensor:

$$\boldsymbol{\sigma} = G\mathbf{M} , \qquad (2)$$

where G is the elastic modulus of the material. The total state of stress of the material is

$$\mathbf{T} = -p\mathbf{I} + \boldsymbol{\tau} + \boldsymbol{\sigma} . \tag{3}$$

This is incorporated in the momentum transport equation for the fluid, which is

$$\frac{\partial \mathbf{u}}{\partial t} = -\mathbf{u} \cdot \nabla \mathbf{u} + \frac{1}{\rho}\left(\nabla \cdot \mathbf{T} + \mathbf{F_b}\right) \tag{4}$$

which is solved along with the mass conservation constraint:

$$0 = \nabla \cdot \mathbf{u} . \tag{5}$$

Both Equations 1 and 4 are solved during each computational cycle where all of the quantities on the right side of the equation were computed during the previous computational cycle. Thus this is an explicit algorithm, and as such, the time step size from one cycle to the next is necessarily limited by numerical stability limits; in the simulations performed here, the limitation was either due to the viscous stress term, or the surface tension computation at the free surface boundary, depending on the capillary number (Ca; the ratio of viscous forces to surface tension forces). Equation 5 is solved implicitly each cycle; the pressure and velocity component at each computational cell are adjusted iteratively until Equation 5 is satisfied to within a convergence criterion. The algorithm automatically adjusts this criterion based on the time step size.

Surface tension and static contact lines

In ***FLOW-3D***®, the free surface is located by the Volume-of-fluid (VOF) technique whereby a colour function is used to predict the regions of the computational domain that are occupied by fluid. The colour function predicts the fractional volume of each computational cell that is occupied by the fluid; the remaining volume (in this work) is presumed to be "void". Unlike many other models that use the VOF method, in ***FLOW-3D***®, the dynamics of the gas phase are not necessarily computed – instead, the model relies on the free surface assumption where the air space's influence on the fluid is merely due to its pressure. This approach alleviates the errors associated with interfacial cells containing two phases of drastically differing densities common to VOF models. The colour function is advected through the domain much like the other flow quantities; however, the model uses special numerical techniques that maintain a sharp interface and limit its numerical diffusion.

At the fluid-air interface, the curvature is calculated from the geometrical distribution of the colour function. The resulting pressure is incorporated into the boundary condition at the free surface.

At contact lines, an additional force describing the adhesion between the solid and the liquid is added to the dynamic processes of mass and momentum conservation. Adhesion forces arise from molecular interactions between the solid and liquid. This interaction is characterized by the static contact angle because the molecular processes that cause the adhesion force act at a space and time scale far smaller and faster than those of the continuum flow process. Therefore, the wall adhesion force is computed from the cosine of the static contact angle and the interfacial tension between the air and the liquid [4]. Imposing this force into the $\mathbf{F_b}$ term of Equation 4 allows the model to dynamically compute an apparent contact angle. For static situations, this will be the apparent static contact angle. For dynamic situations, the apparent contact angle will vary due to the viscous and inertial forces present in the vicinity of the contact line.

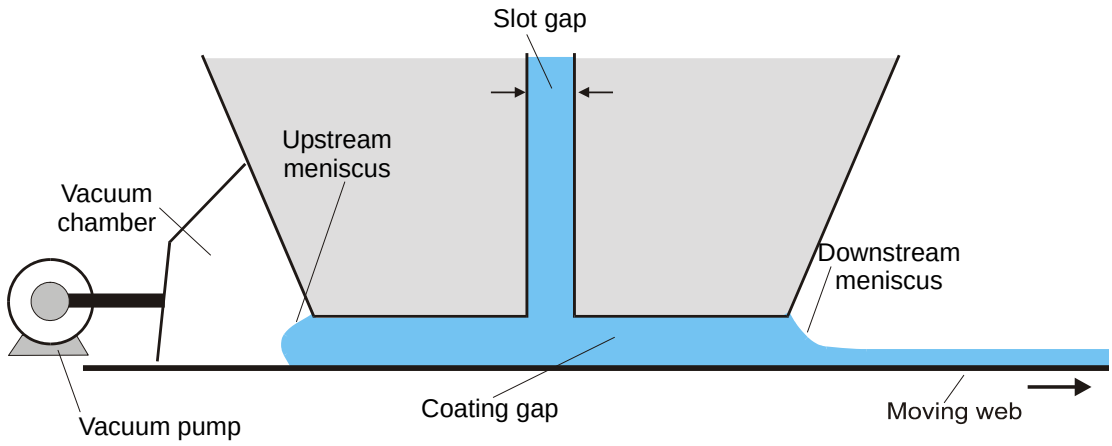

Figure 1: Two-dimensional slice of slot coating process; in the experiments, the coating gap was maintained at 100 μm, the slot gap was 125 μm, and the vacuum pressure and web speed were continously varied.

Low-flow limit in slot coating

The slot coating process is shown in Figure 1. One key operability issue in slot coating is to determine the low-flow limit; this limit is the minimum film thickness that can be stably applied onto a substrate for a given capillary number and the gap between the die and the substrate. This is important because a common goal to slot coating is applying thin films accurately, and maintaining a larger gap is preferred because this layout is less sensitive to variations in the gap during the rotation of the backing roll (roll runout), maintaining a more uniform coating.

Romero *et al* [3] performed experiments to measure the low-flow limit observed during vacuum-assisted slot coating. Their experiments consisted of maintaining a constant web speed while gradually lowering, in steps, the liquid feed to the slot until coating bead failure occurred. The vacuum was also continuously adjusted to maintain the upstream meniscus position (*see* Figure 1). The low-flow limit is reported in terms of the ratio of the coated film to the gap width.

For Newtonian flows, it is been long established that the low-flow limit goes down as the capillary number is lowered; that is, for lower web speeds, lower viscosity, or higher surface tension. Since surface tension is difficult to control, and lower web speeds are antithetical to efficient operation and lower viscosity is obtained with higher solvent loads which must be subsequently dried, this is difficult to achieve. Conversely, higher capillary number flows result in higher low-flow limits. Romero *et al* [3] noted that the presence of elasticity in the flow significantly affected the low-flow limit negatively for the fluids used in their experiments – small concentrations of polyethylene oxide (PEO; molecular weight 8×10^3 g/mol) in a solution of polyethylene glycol (PEG; molecular weight 4×10^6 g/mol) in water. They noted that greater elasticity in the coating medium (i.e. higher elastic modulus, G) tended to raise the low-flow limit for a given capillary number.

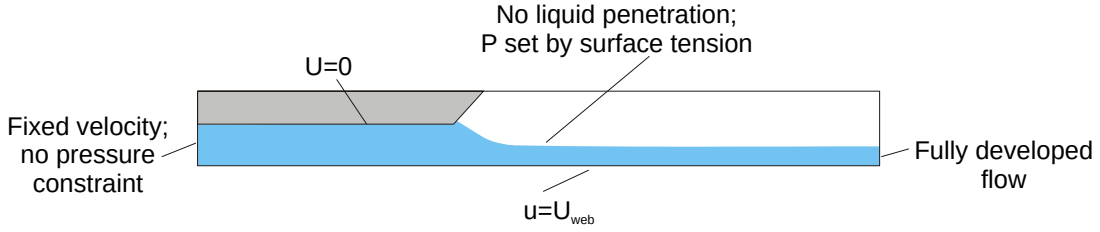

Figure 2: Computational domain and boundary conditions for the two-dimensional flow problem.

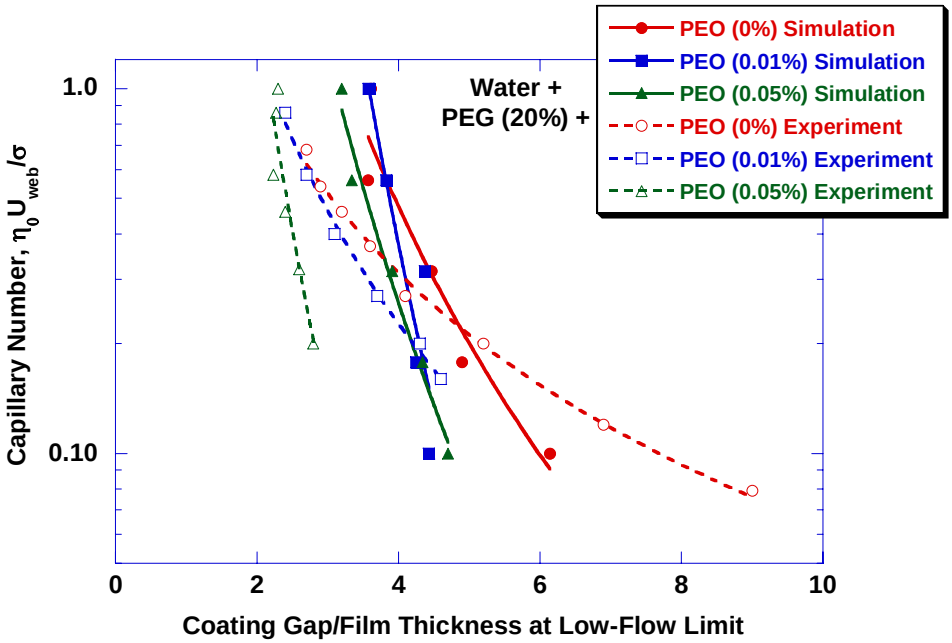

Figure 3: Plot of low flow limits in slot coating as a function of capillary number and fluid elasticity. The solid markers indicate simulation results while the open markers indicate experimental results [3]. The lines represent best-fit power-law curves.

In the simulations performed here, it was deemed that the part of the flow critical to the maintenance of the coating bead was the portion downstream from the slot gap; the flow rate at which the meniscus at the downstream static contact line begins to pull upstream under the die surface is the low-flow limit. Therefore, only the downstream portion of the coating bead was simulated, as the model assumes that the flow entering this part of the domain is fully developed and the imposed vacuum is sufficient to maintain the upstream meniscus. Figure 2 shows the computational domain and boundary conditions that were specified for this simulation. The computational mesh used was a fixed grid in two dimensions composed of 5872 cells (367 in the x-direction by 16 in the y-direction and each mesh cell was 12.5μm square). Table 1 shows the fluid systems considered for the simulations; a solution of 20 wt.% PEG was used with three different concentrations of PEO. The simulations were performed for each fluid system by setting the web speed and then gradually lowering the inflow. The simulated low-flow limit was determined by analyzing the results for the inflow at which the downstream meniscus first begins to pull under the die; the beginning of the coating bead failure was determined by noting the point at which flow reversal began at the downstream meniscus; it is assumed that this reversal would pull the upstream meniscus under the die until air breaks through the coating bead into the vacuum chamber. This was done for a variety of web speeds, and thus capillary number.

Table 1: Properties of coating fluids. All use a 20 wt.% solution of PEG in water as a base.

PEO (wt. %)	η_0 (mPa·s)	G (Pa)	λ (s)
0	17.01	0.00	0.000
0.01	18.86	0.06	0.028
0.05	25.13	0.32	0.025

Figure 3 is a plot of the experimental and computational results of the low-flow limits. The experiments do show a greater effect of the capillary number on the low-flow limit than do the computational results; however, the trends are still valid. In all cases, rising capillary number lowers the gap-to-thickness ratio at the low-flow limit because the shape of the downstream meniscus necessarily changes to account for the lessening of the surface tension effects. Note

also that as the elasticity of the fluid rises, the low-flow limit value shrinks. To understand this realise that the polymer coils in the solution serve to increase the resistance to extensional flow; i.e. they raise the extensional viscosity, and the extensional viscosity rises in flow regions with the greatest extension rates. In slot coating, the greatest extension rates occur at the downstream meniscus. So, increased elasticity acts like the fluid surface is being stretched there, effectively lowering the radius of curvature, which in turn lowers the gap-to-thickness ratio at the low-flow limit.

Possible reasons for the deviation between the experiment and simulation results are:

- Insufficiently fine mesh resolution, especially in the vicinity of the substrate surface. This may cause errors in the calculation of the viscous boundary layer. The evidence for this is the delayed bead breakup at higher Ca. The mesh used was a compromise limited by time constraints.
- Lack of a third dimension. In the experimental analysis, the researchers noted that with the low Ca flows, the flow first became three-dimensional at flow rates greater than the low-flow limit. In the simulations presented here, three-dimensionality was not considered (although ***FLOW-3D***® certainly can allow for this), so it is plausible that the simulations predicted an earlier (*i.e.* at higher inflow) bead breakup and thus a lower low-flow limit value.

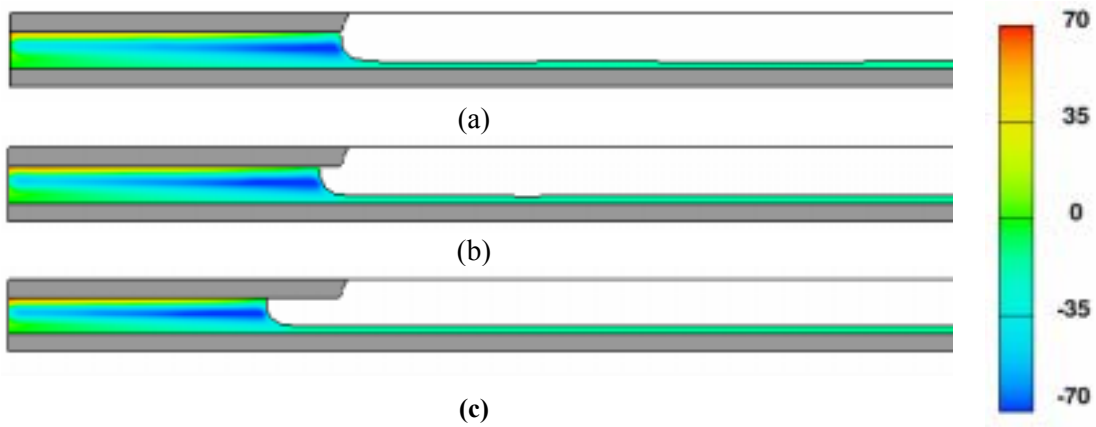

Figure 4: Plots of shear component of elastic stress at the point of bead failure for the case of 0.03 wt.% PEO in a 20 wt.% PEG solution at Ca=0.316. The colour scale at right indicates units in dynes/cm^2.

Three-dimensional curtain coating: edge effects

Although the aforementioned work was performed as a two-dimensional simulation, the algorithm described above is also extended to three dimensions. One example, presented here, is curtain coating. Like slot coating, this is a premetered coating process, but is commonly used where higher web speeds are desired so as to use gravity to provide downward inertia to the coating region to reduce the risk of air entrainment, rather than rely on a vacuum system.

As with slot coating, curtain coating is subject to various defects, one of which is edge defects. At the edge of the curtain, surface tension acts on the sharp curvature present here to retract the curtain in the cross-web direction. This results in a thickening of the applied coating near its edges. In practice, guide wires are commonly employed at these edges to help guide the curtain and minimize the edge defects; however, in the simulations presented here, no guides were considered.

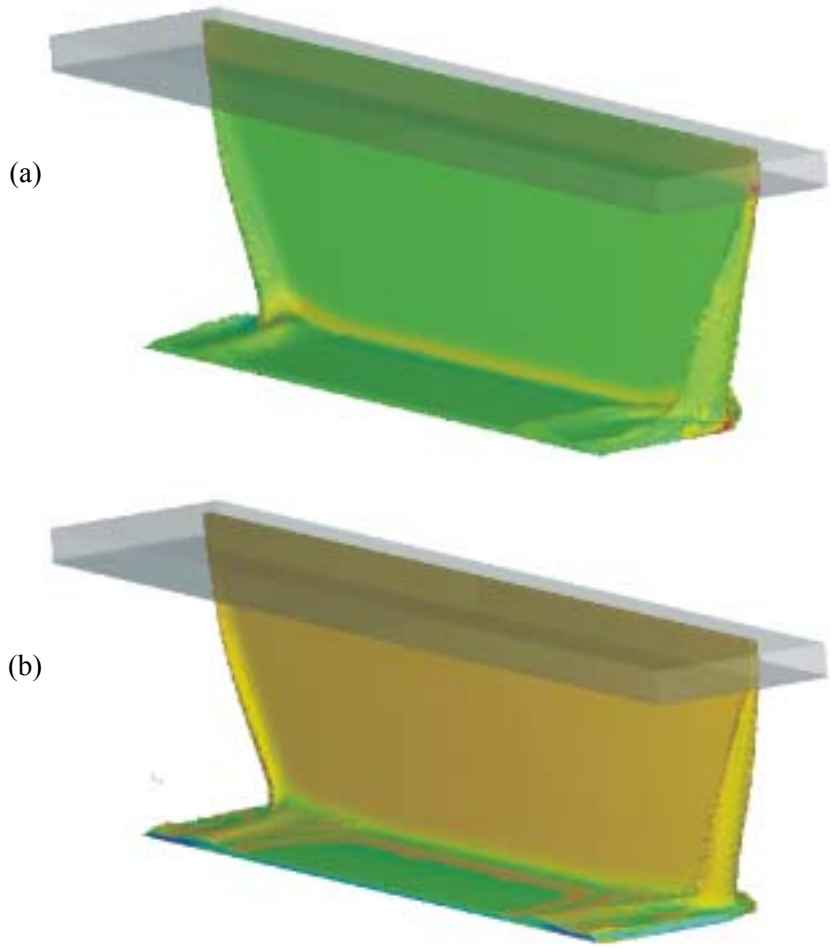

Figure 5 : Image of three-dimensional simulation of curtain coating. Image (a) shows the result for the Newtonian case, while (b) shows the result for the case with a 0.05wt.% PEO solution in a 20wt.% solution of PEG. The colour scale for (a) represents pressure, while for (b) it is the xx-component of elastic stress.

Figure 5 shows the results of these simulations. Case (a) shows the result for the Newtonian flow (the 20wt.% PEG solution – see Table 1 for fluid properties), while case (b) shows the result for the 0.05wt.% PEO in 20wt.% PEG solution. In both cases, the capillary number is 1.3. Note that both cases exhibit edge retraction, as surface tension is significant in both cases. However, in the latter case, the edge retraction appears to be the lesser of the two. Physically, this could be explained by the fact that the deformation due to the retraction is resisted somewhat by the elastic stress. Of course, this is only a small part of the story in curtain coating; this elasticity will also serve to destabilise the upstream contact line at higher web speeds.

Concluding remarks

The ability to simulate elastic properties of materials has been incorporated into a Volume-of-Fluid (VOF) computational fluid dynamics algorithm. Currently available is a model to simulate solidified and Bingham-like materials, which includes advection, translation, rotation and yielding in the computation of the elastic stress tensor components. This work expands on this by considering a conformation tensor approach and relaxation of the material, and represents preliminary work not yet available in ***FLOW-3D***®. The results here show great promise for the model, and continuing work will enhance the model with more constitutive relations, greater flexibility and more numerical options to reduce computation time.

References

1. ***FLOW-3D***® is developed by and is a trademark of Flow Science, Inc., Santa Fe, N. Mex., USA.
2. M. Pasquali, L.E. Scriven. Free surface flows of polymer solutions with models based on the conformation tensor. *J. Non-Newtonian Fluid Mech*. **108** (2002) 363-409.
3. O. J. Romero, W. J. Suszynski, L. E. Scriven and M. S. Carvalho. Low-flow limit in slot coating of dilute solutions of high molecular weight polymer. *J. Non-Newtonian Fluid Mech.* **118** (2004) 137-156.
4. Young, T., An essay on the cohesion of fluids, *Phil. Trans. Royal Soc.* (London), **95** (1805) p. 65.